Comptes Rendus

Chimie

Dominique Bazin, Robert J. Papoular, Erik Elkaim, Raphael Weil,
Dominique Thiaudière, Céline Pisapia, Benedicte Ménez, Nathaniel
S. Hwang, Frederik Tielens, Marine Livrozet, Elise Bouderlique,
Jean-Philippe Haymann, Emmanuel Letavernier, Louis Hennet,
Vincent Frochot and Michel Daudon

**Whitlockite structures in kidney stones indicate infectious origin: a
scanning electron microscopy and Synchrotron Radiation investigation**

Microcrystalline pathologies: Clinical issues and nanochemistry / *Pathologies microcristallines : questions cliniques et nanochimie*

Whitlockite structures in kidney stones indicate infectious origin: a scanning electron microscopy and Synchrotron Radiation investigation

La relation à l'infection pour les calculs rénaux contenant la whitlockite : une étude physicochimique basée sur des techniques associées au rayonnement synchrotron

Dominique Bazin[*],[a], **Robert J. Papoular**[b], **Erik Elkaim**[c], **Raphael Weil**[d], **Dominique Thiaudière**[c], **Céline Pisapia**[e], **Benedicte Ménez**[e], **Nathaniel S. Hwang**[f], **Frederik Tielens**[g], **Marine Livrozet**[h,i], **Elise Bouderlique**[h,i], **Jean-Philippe Haymann**[h,i], **Emmanuel Letavernier**[h,i], **Louis Hennet**[j], **Vincent Frochot**[h,i] **and Michel Daudon**[h,i]

[a] Université Paris-Saclay, CNRS, Institut de Chimie Physique, 310 rue Michel Magat, 91400 Orsay, France

[b] Saclay Institute for Matter and Radiation (IRAMIS), Laboratoire Léon Brillouin, CEA-Saclay, 91191 Gif sur Yvette Cedex, France

[c] Synchrotron SOLEIL, L'Orme des Merisiers, Saint-Aubin - BP 48, 91192 Gif-sur-Yvette Cedex, France

[d] Université Paris-Saclay, CNRS, Laboratoire de Physique des Solides, Université Paris Sud, 91400 Orsay, France

[e] Université de Paris, Institut de physique du globe de Paris, CNRS - 1, rue Jussieu - 75238 Paris Cedex 05, France

[f] School of Chemical and Biological Engineering, NBio Institute, Institute of Chemical Processes, Seoul National University, Seoul, 151-744, Republic of Korea

[g] General Chemistry (ALGC) - Materials Modelling group, Vrije Universiteit Brussel (Free University Brussels-VUB), Pleinlaan 2, 1050 Brussel, Belgium

[h] INSERM, UMRS 1155, Sorbonne Université, Hôpital Tenon, 75020 Paris, France

[i] Service d'explorations fonctionnelles, Hôpital Tenon, AP-HP, 4, rue de la Chine, 75020 Paris Cedex 20, France

[j] ICMN, UMR7374, CNRS, 45071 Orléans Cedex 2, France

_____

[*] Corresponding author.

E-mails: dominique.bazin@universite-paris-saclay.fr (D. Bazin),
robert.papoular@cea.fr (R. J. Papoular), erik.elkaim@synchrotron-soleil.fr (E. Elkaim),
raphael.weil@u-psud.fr (R. Weil), dominique.thiaudiere@synchrotron-soleil.fr
(D. Thiaudière), pisapia@ipgp.fr (C. Pisapia), menez@ipgp.fr (B. Ménez),
nshwang@snu.ac.kr (N. S. Hwang), frederik.tielens@vub.be (F. Tielens),
Marine.livrozet@aphp.fr (M. Livrozet), Eliseboud@aol.com (E. Bouderlique),
jean-Philippe.haymann@aphp.fr (J.-P. Haymann), emmanuel.letavernier@aphp.fr
(E. Letavernier), louis.hennet@cnrs-orleans.fr (L. Hennet), vincent.frochot@aphp.fr
(V. Frochot), michel.daudon@aphp.fr (M. Daudon)

Abstract. In this contribution dedicated to kidney stones containing Whitlockite (Wk), we addressed three questions, namely, the presence of iron in Wk, the relationship between bacterial imprints and the presence of Wk, and finally the relationship between the crystal size of Wk-bearing stones and infection. The complete dataset indicates that iron is not present in our Wk stoichiometry. We also note the presence of bacterial imprints for kidney stones with a high, but sometimes a low content, of Wk. Finally, we propose FE-SEM as a diagnostic tool for stone patients who have a negative urine culture associated with kidney stones containing less than 20% by weight Wk, a low level of carbonate in apatite, and no struvite. Such a diagnostic tool would represent a significant benefit to the clinician.

Résumé. Dans cette contribution, nous étudions les calculs rénaux contenant la whitlockite (Wk). En premier lieu, la présence du fer dans la formule stœchiométrique de la Wk est discutée grâce à la fluorescence X. Puis, nous abordons la relation à l'infection à l'aide d'observations au Microscope électronique à balayage (MEB) aptes à mettre en évidence de possibles empreintes de bactéries. Elles montrent que le processus infectieux est établi pour des teneurs supérieures à 20%, ceux-ci ne pouvant toutefois pas être écartés en dessous de cette teneur. Finalement, l'étude de relation entre la taille des cristaux de Wk et l'infection par DRX ne permet pas de l'établir. Le message pour le clinicien est le suivant : pour un patient asymptomatique, si le calcul ne contient ni struvite, ni apatite carbonatée et moins de 20% de Wk, il convient d'observer par MEB les calculs rénaux afin de pouvoir écarter ou non un processus infectieux.

1. Introduction

Numerous studies have underlined a significant global increase in prevalence and incidence of nephrolithiasis [1–4]. Part of this increase is related to the relationship between urolithiasis and major public health problems such as metabolic syndrome [5,6]. Urinary tract infection (UTI) leading to the formation of kidney stones can also be considered a relevant factor [7,8]. In view of the increase in infection-related stones over the past two decades, UTI must always be considered a significant possible cause of urolithogenesis [9–13].

Several kidney stone chemical phases are related to kidney infection [14–18]. Among them we can cite calcium phosphate apatite with a high level of carbonate [19–21], ammonium urate [22], struvite [23–26] and whitlockite (Wk) [27,28]. High carbonate calcium phosphate apatite and struvite are related to urease-producing bacteria, while Wk may be related to infection by non-urease-producing bacteria. There is another major difference between struvite and Wk. While the presence of struvite (independently of its weight fraction) is directly related to infection, the weight fraction of Wk in kidney stones, estimated by Fourier transform infrared spectroscopy (FTIR), was related to infection with a high degree (80%) of statistical significance if greater than 20% [15].

For further insight into the relationship between infection and kidney stones containing Wk without struvite, we have used physicochemical characterization techniques [29–32] to obtain a precise multiscale description of such concretions [33–37]. First, by analogy with geological studies [38], we assessed the presence of iron in Wk by X-ray fluorescence (XRF) [39–41] using synchrotron radiation (SR) as a probe [42–46]. Iron in Wk may modify the position of IR absorption bands and thus may confuse the analysis of IR spectra. Then, we address the size of Wk nanocrystals for an initial set of infection-related kid-

ney stones containing more than 20% Wk in weight, using SR-wide angle X-ray scattering (WAXS) [47–52]. We use the definition of the terms "nanocrystals" and "crystallites" of Van Meerssche and Feneau-Dupont, i.e. crystallites (typically measuring tens of micrometres) composed of accretions of nanocrystals (typically measuring hundreds of nanometres), to describe the structural hierarchy of pathological calcifications [53].

For the first set of kidney stones, field emission scanning electron microscopy (FE-SEM) observations allowed precise crystallite definition in order to ultimately pinpoint bacterial imprints. For the second set, containing less than 20% by weight Wk, FE-SEM was also performed for bacterial imprints to establish a possible infection process. Such a multiscale approach taking into account chemistry and morphology has already been used to develop new diagnostic tools, or to deduce the very first steps of calcification pathogenesis [54–59].

2. Materials and methods

2.1. *Samples*

Kidney stones (Tenon Hospital) from 31 patients (12 males, 19 females) were investigated (see Tables 1 and 2).

2.2. *Investigational tools*

Initial analysis was carried out at the hospital using a stereomicroscope for morphological typing and a FTIR spectrometer to accurately determine stone composition [60–63]. FT-IR experiments were performed in transmission mode using a FTIR spectrometer Vector 22 (Bruker Optics, Marne-la-Vallée, France) covering the mid-infrared range from 2.5 to 25 µm.

A Zeiss SUPRA55-VP scanning electron microscope with an energy-dispersive X-ray (EDX) spectrometer was used for direct microstructure observation. Images were obtained without any conductive coating on the sample. This field emission gun microscope can operate at 0.5–30 kV accelerating voltage. High resolution observations were obtained around 1 kV using two secondary electron detectors: an in-lens and an Everhart–Thornley detector [64]. Note that such observations allow the clinician to
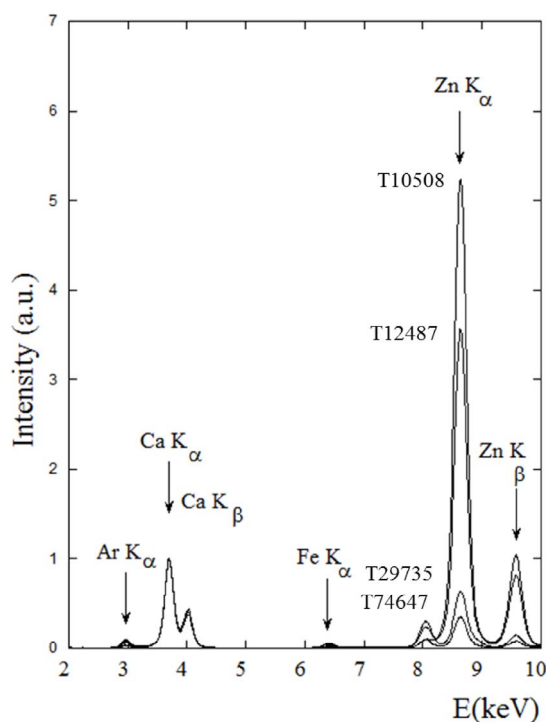

Figure 1. Normalized X-ray fluorescence spectra (the contribution of Ca is set to 1) collected for different kidney stones (T10508, T12487, T29735, T74647) containing Wk. The contributions of Ca ($K_\alpha = 3.691$ keV, $K_\beta = 4.012$ keV), Zn ($K_\alpha = 8.638$ keV, $K_\beta = 9.572$ keV) are clearly visible. Note the absence of a significant contribution from possible iron.

determine the morphology of crystallites which is a major parameter in nephrology [65–68].

One set of X-ray fluorescence experiments as well as three sets of X-ray scattering measurements were conducted at the synchrotron facility SOLEIL (Saint-Aubin, France). The X-ray fluorescence experiments were carried out at the Diffabs beamline (e.g. Figure 1). The main optical system includes a fixed-exit double crystal monochromator composed of two independent Si(111) crystals and located between two long mirrors (50 nm Rh-coated Si) [25].

The X-ray scattering experiments were performed at the Cristal beamline during two consecutive SOLEIL synchrotron sessions, using first a 18.446 keV ($\lambda = 0.67212$ Å) and then a 17.017 keV ($\lambda = 0.72857$ Å) monochromatic beam. Note that the monochroma-

Table 1. Clinical data for the first set of kidney stones containing more than 20% in weight of Wk and related to infection

	Sex, age (year)	Location	Chemical composition estimated through FTIR	Carbonate level	Crystal size estimated through WAXS
T10508	F, 59	Staghorn_Kidney	38% CA, 28% Wk, 20% glafenic acid, 10% Prot, 4% C1	/	
T12487	F, 54	Ureter	50% CA, 23% Wk, 20% C1, 7% Prot	5%	/
T12900	M, 55	Kidney	35% CA, 25% Wk, 25% ACCP,10% C1,5% Prot		
T17405	M, 65	Kidney	50% CA, 25% Wk, 20% ACCP, 5% Prot	19%	/
T17615	M, 36	Bladder	40% CA, 28% Wk, 26% ACCP, 4% Prot, 2% C2		
T29735	F, 59	Urinary tract	30% CA, 25% Wk, 20% ACCP, 15% Prot, 5% TGL, 5% C2	19%	/
T32616	F, 22	Kidney	30% Wk, 21% C1, 20% CA, 15% C2, 7% Prot	7%	290 nm ± 10 nm
T38693	M, 52	Staghorn	35% Wk, 24% C1, 19% CA, 16% C2, 8% Prot	7%	/
T38952	M, 3	Urethra	40% Wk, 13% C1, 20% CA, 15% ACCP, 5% C2, 7% Prot	5%	90 nm ± 10 nm
T43068	F, 54	Kidney	66% Wk, 19% CA, 9% Prot, 6% C1	/	30 nm ± 10 nm
T43736	M, 4	Kidney	67% Wk, 3% C1, 20% CA, 10% Prot	6%	250 nm ± 10 nm
T44112	M, 87	Expelled	42% Wk, 20% C1, 20% CA, 11% C2, 7% Prot	7%	/
T45449	F, 39	Ureter	75% Wk, 12% Prot, 8% CA, 3% C1, 2% TGL	/	330 nm ± 10 nm
T51263	M, 70	Urinary tract	75% Wk, 12% Prot, 10% CA, 3% C1	/	330 nm ± 10 nm
T52975	F, 89	Urinary tract	60% Wk, 25% CA, 10% Prot, 5% TGL	10%	130 nm ± 10 nm
T55785	F, 54	Kidney	50% Wk, 7% C1, 33% CA, 10% Prot,	5%	190 nm ± 10 nm
T58866	F, 77	Tubular	52% Wk, 25% CA, 15% ACCP, 8% Prot,	25%	/
T71739	F, 69	Kidney	45% Wk, 25% CA, 22% ATZ 8% Prot,	/	/
T74647	F, 72	Ureter	75% Wk, 20% CA, 5% Prot	8%	90 nm ± 10 nm
T74808	M, 34	Prostate urethra	26% Wk, 21% C2, 17% Br, 14% CA, 10% OCP, 7% Prot, 3% C1, 2% TGL	6%	120 nm ± 10 nm

Wk = whitlockite; Br = brushite; CA = carbonated calcium apatite; C1 = whewellite; C2 = weddellite; ACCP = amorphous carbonated calcium phosphate; Prot = protein; TGL = triglycerides; ATZ = atazanavir; OCP = octacalcium phosphate.

tor was calibrated using a standard LaB_6 powder (NIST SRM 660b). The samples, introduced in kapton capillaries (ø = 0.7 mm), were mounted on a spinner rotating at 5 Hz to improve particle orientational averaging. Data were collected in Debye–Scherrer mode using a 21 Si(111) crystal analyser. With this setup and for each sample, two high angular resolution diagrams recorded in about one hour were summed since sample degradation under the X-ray beam was not significant (Figure 2). Details regarding the experimental set up can be found in reference [69]. To allow for their subsequent superimposition in the same figures, all the collected X-ray diffractograms were first preprocessed using the freely available Graphical User Interface WIN-PLOTR software [70]. The mean size of the coherently diffracting crystals was calculated using the GSAS software [71].

3. Results and comments

As emphasized by Borghi *et al.* [72], the relationship between nephrolithiasis and urinary tract infections is complex and difficult to analyse both from a pathophysiological and clinical point of view. This has prompted several investigations to understand the relationship between infection and urinary stones [73,74], most of them focussing on struvite [75–81]. Here we attempt to broaden the scope of studies of this pathogenesis by describing in detail the physicochemical characteristics of stones containing Wk without struvite. At this point, it is worth bearing in mind that Wk has been reported in different parts of the body including lungs [82], breast [83], gallstone [84], prostate [85,86], aorta [87],

Table 2. Clinical data related to the second set of struvite-free kidney stones containing less than or equal to 20% in weight of Wk and a low carbonate level for the apatite

	Sex, age (year)	Location	Chemical composition estimated through FTIR	Apatite carbonate level
T3347	M, 86	Bladder	70% CA, 15% Wk, 10% C2, 5% C1	9%
T4216	F, 31	Ureter	60% C2, 20% CA, 12% Wk, 8% Prot	/
T9261	M	Bladder	69% CA, 18% Wk, 8% C2, 3% C1, 2% Prot	8%
T9491	F, 43	Ureter	55% CA, 18% C1, 15% Wk, 8% Prot	3%
T10410	M, 65	Kidney	61% CA, 16% Wk, 15% C1, 8% Prot	6%
T11564	F, 40	Urinary tract	70% CA, 15% Wk, 7% C2, 5% OCP, 3% C1	7%
T11866	F, 58	Ureter	35% CA, 33% C1, 17% Wk, 15% C2	6%
T18382	F, 34	Ureter	52% CA, 30% C1, 14% Wk, 4% Prot	4%
T22610	F, 68	Kidney	45% CA, 20% Wk, 17% C1, 10% Prot, 8% ACCP	/
T33101	F, 50	Kidney	45% CA, 30% C1, 18% Wk, 7% Prot	10%

Wk = whitlockite; Br = brushite; CA = carbonated calcium apatite; C1 = whewellite; C2 = weddellite; ACCP = amorphous carbonated calcium phosphate; Prot = protein; TGL = triglycerides; ATZ = atazanavir; OCP = octacalcium phosphate.

bone [88], cartilage [89] and salivary glands [90], and to note that emerging evidence indicates that bacteria are present in and contribute to other calcifications such as vascular calcification [91].

Wk has also been identified as a kidney stone component [92–94]. While several publications concentrate on kidney stones containing struvite, little is known regarding the relationship between infection and kidney stones containing Wk. Interestingly, hyperthermophilic bacteria (70–110 °C) have been shown to be able to convert an amorphous calcium phosphate phase into fully crystalline Wk mineral, and spherulitic clusters that we interpret to be hydroxyapatite-like nanocrystals [95].

One of the various geological studies of Wk [96–98] underlines the presence of iron in the crystallographic structure [38]. To assess the presence of this element in Wk of biological origin, we began our investigation with SR-XRF experiments. Figure 1 shows X-ray fluorescence spectra of different kidney stones. The presence of Ca as well as Zn has been already discussed [44,45,99–102]. Note that although the Zn signals are more prominent than those of Ca, it doesn't indicate higher Zn content. Various correction procedures have to account for the self-absorbing matrix and the fact that measurements have been performed in air, the nature of the matrix, absorption by air, incident beam energy, and the ion-

ization and X-ray emission cross-sections associated with each element [103,104]. In our case, the experiment was optimized for the X-ray fluorescence of Zn (K_α = 8.638 keV, K_β = 9.572 keV).

As the majority of the fluorescence events arise from photons with energy just above the absorption edge, the SR-XRF sensitivity is optimized for elements with X-ray fluorescence lines just below the monochromatic excitation energy, which in this case is Zn. In addition, X-ray production cross-sections are a function of Z^4 for SR-XRF, where Z is the atomic number of the target element. Finally, characteristic Zn X-ray emissions occur at higher energy than those of Ca (K_α = 3.691 keV, K_β = 4.012 keV), which is thus more susceptible to absorption and significantly affected by air between the sample and the detector.

The intensity of Zn X-ray fluorescence seems to be related to the carbonated calcium apatite (CA) content. High intensity values correspond to samples with a high CA content (38% CA for 10508, 50% CA for T12487) and weak ones to lower (30% CA for 29735, 20% CA for T74647). Note the weak signal for Zn X-ray fluorescence for sample T74647 which contains 75% by weight Wk. In all these measurements the absence of a significant contribution from iron is striking, implying the stoichiometric formula $Ca_9Mg(HPO_4)(PO_4)_6$ for kidney stones con-

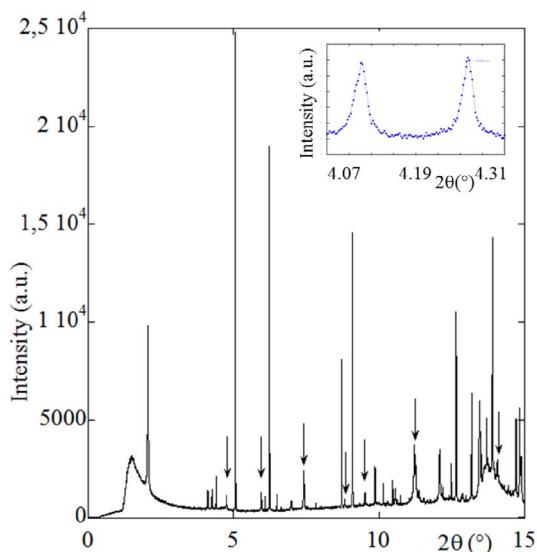**Figure 2.** Typical high resolution X-ray powder diffractogram measured on the Cristal beamline for sample T74808 ($\lambda = 0.67212$ Å). The whitlockite diffraction peaks are marked with an arrow. Note the prominent 010 reflection of the octacalcium phosphate (OCP) crystalline phase, which occurs at $2\theta = 2.051°$ and two other Bragg reflections [100,110] pertaining to OCP for $2\theta = 4.117°$ and $4.261°$, respectively (see inset). Note that the associated OCP phase has only been detected by FTIR spectroscopy through detailed analysis based on spectral derivatives. OCP indicates possible hypercalciuria without any link with infection. Accordingly, we will not discuss the presence of this compound further.

Figure 3. Sample T51263 (75% Wk, 12% Prot, 10% CA, 3% C1) (a) characteristic pseudocubic morphology of Wk as seen by FE-SEM and corresponding EDX spectrum (b) in which the contributions of C ($K_\alpha = 0.277$ keV), O ($K_\alpha = 0.525$ keV), Mg ($K_\alpha = 1.253$ keV), P ($K_\alpha = 2.014$ keV), and Ca ($K_\alpha = 3.691$ keV, $K_\beta = 4.012$ keV) are clear. Note the presence of a sum peak (SP) due to the coincidence of two O K_α photons.

taining Wk.

Iron is an element of considerable biological importance due instance to its presence in major proteins such as haemoglobin, and links to some genetic diseases; for this reason we have already proposed the use of X-ray fluorescence to detect it in biological tissue [105,106]. It is quite clear that there is no iron in the stoichiometric formulation of biological Wk.

Next, SEM observations were made on kidney stones with high Wk content; these (Figure 3a) clearly show pseudocubic crystallites with a trigonal geometry. Associated EDX spectra shows contributions of the different elements in the Wk stoichiometric for-
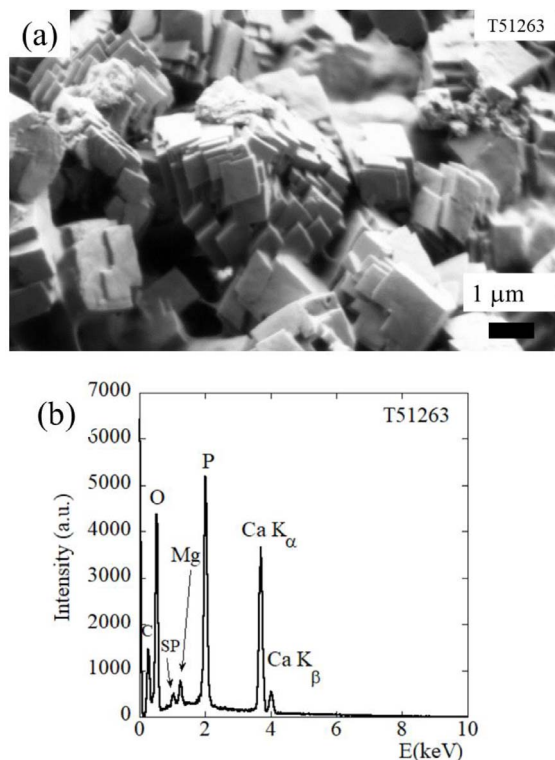
mula $Ca_9Mg(HPO_4)(PO_4)_6$, namely O, P, Mg and Ca (Figure 3b). One interesting fact lies on the morphology of Wk crystallites.

According to Frondel [96], crystals are usually simple rhombohedra as shown in Figure 4a, but are sometimes modified by small faces as shown in Figure 4b. Here, we have always observed the first one (white arrows on Figure 4c). However, in the case of synthetic Wk [107,108] as well as in the case of breast cancer, the second morphology was observed (white arrows on Figures 4d,e). It seems thus that in the case of infection, the local biochemical environment defined by the kidney and/or by the bacteria induce the formation of Wk crystallites with a pecu-
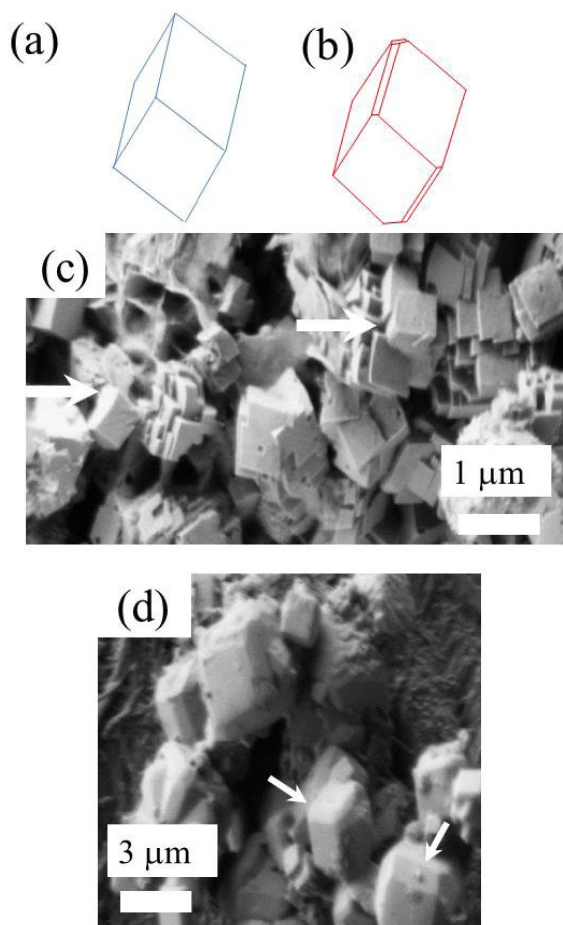
Figure 5. Bacterial imprints (red arrows) observed close to Wk crystallites (white arrow).
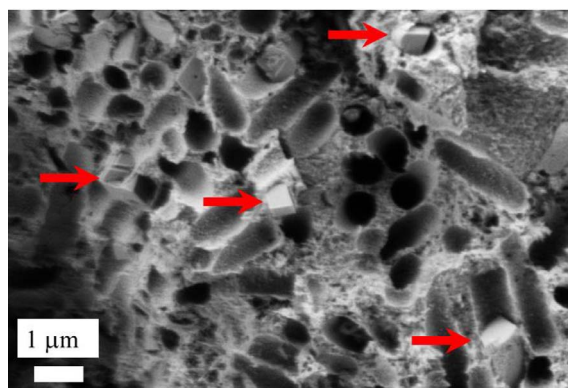
Figure 6. Wk crystallites (red arrows) present in bacterial imprints.

Figure 4. (a, b) The morphologies for Wk crystals. Reprinted from [96], with the permission of Mineralogical Society of America. (c) SEM observation of the Wk part of kidney stones related to infection. (d) SEM observation of breast calcifications made of Wk.

liar morphology.

The mineralogical composition of the kidney stones as given by FTIR spectroscopy (Tables 1 and 2) explains the presence of carbon (Figure 3b). In kidney stones containing a high level of Wk, bacterial cell imprints are clearly visible at the surface of and probably within the apatitic part of the kidney stones (red arrows in Figure 5) but not at the surface of Wk crystallites (white arrow on Figure 5) [109].

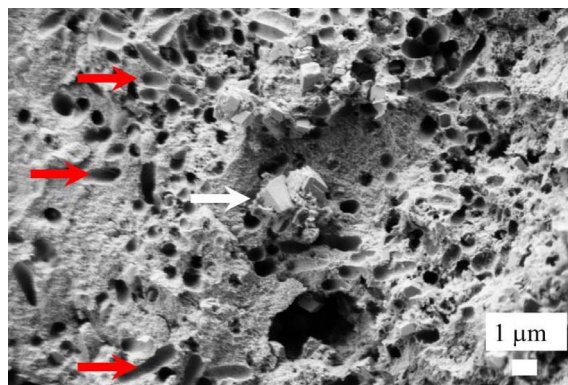Finally, at higher magnification, it is possible to observe Wk crystallites in bacterial imprints (red arrows on Figure 6). Such an observation is consistent with the fact that, as previously emphasized, an intimate link exists between Wk and bacteria [15].

In some kidney stones, FE-SEM did not reveal a large number of automorphic Wk crystallites. Instead some microscale crystallites were observed (red arrows on Figure 7a) in which EDX clearly shows contributions from Mg (Figure 7b).

The second part of this investigation on the first set of kidney stones (with Wk content greater than 20% by weight) focuses on the size of the Wk nanocrystals, characterized using high resolution X-ray powder diffraction on selected examples (Figure 2).

For one sample, it was possible to measure the mean size of the coherently diffracting crystals. For the other samples, we used the Scherrer formula
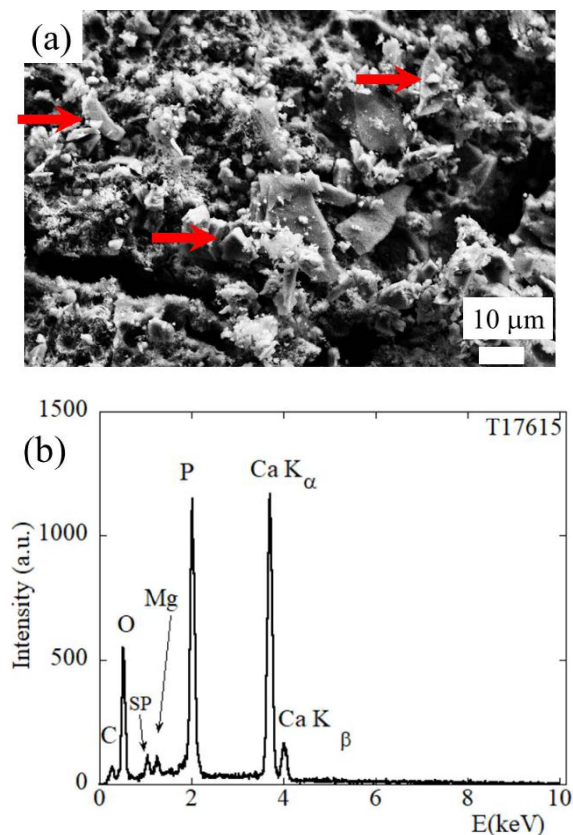
Figure 7. Sample T17615 (40% CA, 28% Wk, 26% ACCP, 4% Prot, 2% C2) (a) Wk (red arrows) as observed by its trigonal morphology in FE-SEM, and corresponding EDX spectrum (b) showing contributions from C (K_α = 0.277 keV), O (K_α = 0.525 keV), Mg (K_α = 1.253 keV), P (K_α = 2.014 keV), Ca (K_α = 3.691 keV, K_β = 4.012 keV). Note the presence of a sum peak (SP) due to the coincidence of two O K_α photons.

[110,111] $D(2\theta) = K\lambda/L\cos(\theta)$, a relationship between $D(2\theta)$, the diameter of the crystallites, and the width of the scattering peak L. Note that K is a dimensionless geometrical factor of the order of 1 related to the specific shape of the targeted nanocrystal. As reported previously, this factor was set to unity in our evaluation of the crystal size [112].

Such simple analysis supposes similar peak broadening due to microstrain for all the samples and an isotropic morphology for the Wk crystals (which is the case for the automorphic crystals) [113]. Figure 8 shows that the scattering peak characteristic
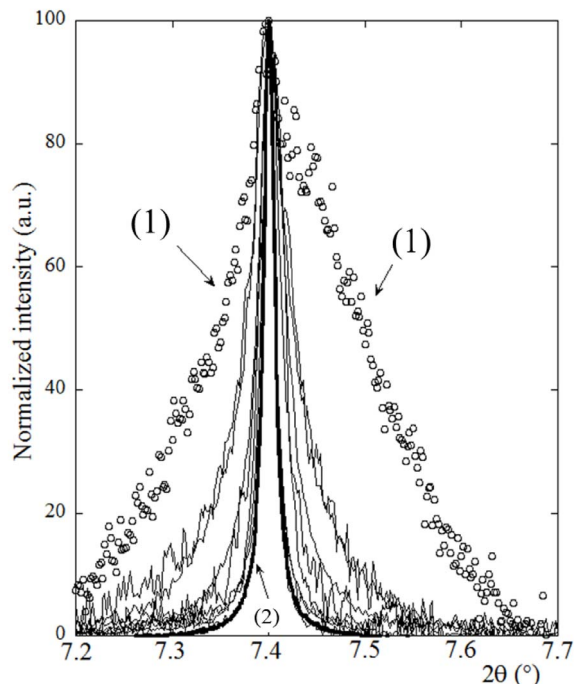

Figure 8. Widths of the Wk-specific scattering Bragg peak (2 −1 0 reflection, d = 5.165 Å) for those kidney stones measured. Note in particular: (1-white circle) = T43068 (66% Wk), (2-bold solid line) = T51263 (75% Wk). Note that the wavelength chosen to superimpose all X-ray diffractograms is 0.67212 Å, as in Figure 2.

of Wk in the different experimental diffractograms displayed very different widths. In fact, it was impossible to investigate kidney stones with lower Wk content using X-ray scattering, suggesting that Wk exists in an amorphous state in low Wk content stones.

Table 1 shows that the size distribution of the Wk nanocrystals is quite large, which may be a function of various chemical parameters such as pH and ionic concentration as shown in a recent investigation of struvite [114]. These results seem to indicate that there is no specific size for the Wk crystals when there is an infection.

To understand the relationship between Wk in kidney stones, and infection, the foregoing structural description of Wk has to be complemented by chemical information. The ratio of Mg/Ca in stoichiometric Wk is 0.0643. In urine, this ratio is around 0.4 if we consider that normal calcium excretion is around 5 mmol/day and magnesium excretion is

around 2 mmol/day. The normal value for phosphate is around 20 mmol/day, so all the elements present in the stoichiometric formula of Wk are present and so Wk biogenesis may well occur alongside that of CA.

In fact, the formation of CA as well as Wk requires destabilisation of the water molecules around the Ca^{2+} and Mg^{2+} cations. Based on molecular dynamics simulations using a polarizable potential, Jiao *et al.* [115] have shown that the lifetime of water molecules in the first solvation shell of Mg^{2+} is on the order of hundreds of picoseconds, in contrast to only a few picoseconds for Ca^{2+}, K^+, or Na^+. Such a simulation indicates that the stability of water molecules around Mg^{2+} is higher than the one around Ca^{2+}, favouring the formation of CA over Wk, the formation of the first one is hence favoured. To promote the formation of Wk, the first hydration shell of Mg^{2+} cations has to be destabilized. We propose that this may be achieved by physisorption of Mg^{2+} at the surface of bacteria [116].

Several points lead to the proposition that bacteria may play a key role in this destabilization process. Firstly, among one hundred chemical phases identified in kidney stones only two common ones contain Mg^{2+}, namely struvite and Wk, and these two chemical phases are related to infection. Secondly, Mg^{2+} cations play a key role in bacterial metabolism [117,118]. Finally, we have observed Wk crystallites inside bacterial imprints. These facts indicate the possibility of destabilization of the Mg^{2+} hydration shell by bacteria. Note that such a hypothesis also implies that for bacteria with urease, the decomposition of urea constitutes a much favourable pathway, leading to the formation of struvite and highly carbonated apatite, than the formation of Wk.

Finally, we consider a set of kidney stones (Table 2) with Wk content equal to or less than 20% by weight. In some samples, bacterial imprints were observed along with Wk crystallites, as in sample T3347 (Figure 9a). For other stones, no bacterial imprints, or Wk crystallites, could be detected (Figure 9b). Even though our sample number is quite low, this suggests that in the case of infection, Wk crystallites are observed. Otherwise, Wk may be present but in an amorphous state.

What is the benefit of these investigations to the clinician? Firstly, we confirm that kidney stones containing more than 20% by weight of Wk are related
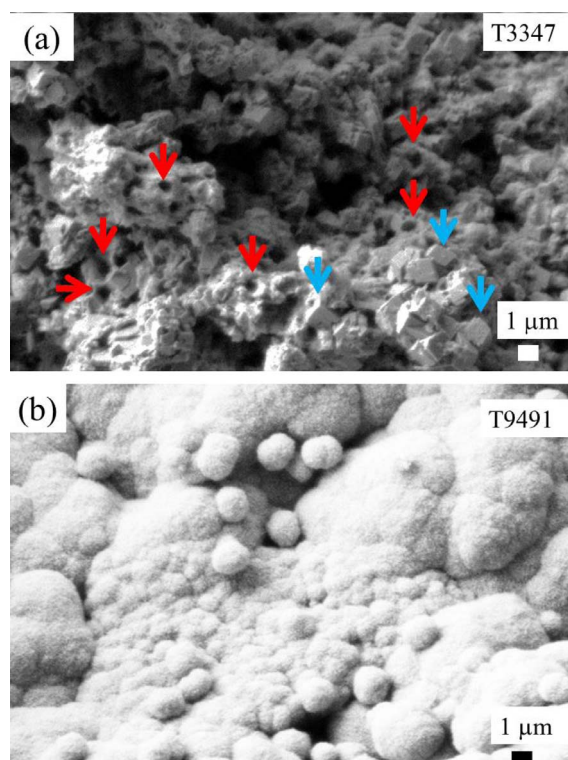

Figure 9. (a) For sample T3347 (15% by weight), very small Wk crystallites (blue arrows) as well as bacterial imprints (red arrows) are observed. (b) Bacterial imprints and Wk crystallites are not observed for the sample T9491 (Wk-free based on FTIR estimates).

to infection. This is consistent with previous studies which indicate a content of 25% in weight of Wk [15]. Second, this study proposes a new approach for the characterization of kidney stones containing less than 20% by weight of Wk, a low level of carbonate in apatite, and no struvite, in patients presenting a negative urine culture. At this point, we must underline that according to the data gathered in our laboratory, which are based on the analysis of 70,728 kidney stones, 3171 kidney stones contain Wk. Among these, 1728 contain less than 20% in weight of Wk, a low level of carbonate in the apatite and no struvite, and are associated with a negative urine culture. For these 1728 stones, which correspond to 2.5% of the patients, the relationship with infection is not clear. In the present instance, we found that 4 stones out of a set of 11 presented bacterial imprints

by FE-SEM.

We propose that, for these patients, FE-SEM could represent a significant diagnostic tool able to disclose possible infection. If FE-SEM underlines the presence of bacterial imprints, there are two possibilities to explain such observation. Is the stone linked to previous infection? In that case the clinical data doesn't contain such information and it is of primary importance to have such information regarding etiology. Is the stone linked to present infection? In that case, the lithogenic process is active for the patient and antibiotic have to be given. In both cases, it is clear that FE-SEM bring major information to the clinician.

We propose thus that for patients having kidney stones without struvite, carbapatite with a low level of carbonate and a low content of Wk, FE-SEM could represent a significant diagnostic tool able to disclose possible infection.

4. Conclusion

These investigations focused on kidney stones containing Wk, a mineral closely correlated with bacterial infection when its content is greater than 20% by weight by FTIR spectroscopy. Firstly, we stress that iron is not present in Wk when the latter occurs in kidney stones. Secondly, FE-SEM supports the relationship between Wk and infection. Bacterial imprints were observed in all the kidney stones containing higher than 20% by weight Wk. Moreover, WK related to infection seems to have a specific morphology. Thirdly, a measurement of Wk crystal size has been performed by X-ray diffraction based on the width of a specific diffraction peak (i.e. [210]). A detailed analysis of the high resolution X-ray powder diffratograms indicates a large distribution of crystal sizes between samples. It seems thus that Wk content, but not crystal size, in kidney stones correlates with infection. Finally, based on FE-SEM observations as well as molecular dynamics' simulations, we propose that bacteria are able to destabilize the first hydration shell of Mg^{2+} cations. For bacteria with urease, the decomposition of urea to ammonia provides a more favourable chemical pathway, to struvite and carbonated apatite, than to Wk.

In conclusion, we propose FE-SEM as a diagnostic tool for patients with kidney stones containing less than 20% Wk, a low level of carbonate in apatite,

without struvite, and with a negative urine culture. FE-SEM observations will give direct evidence of bacterial imprints at the surface. These may eventually be observed through tomography, if experimental configurations such as Nanoscopium [119,120] or Anatomix [121] are able to deal with biological samples with low acquisition time and submicrometer spatial resolution.

Acknowledgments

References

[1] M. Daudon, *Annales d'urologie*, 2005, **39**, 209.

[2] V. Romero, H. Akpinar, D. G. Assimos, *Rev. Urol.*, 2010, **12**, article no. e86.

[3] T. Knoll, *European Urology Supp.*, 2010, **9**, 802.

[4] I. Sorokin, C. Mamoulakis, K. Miyazawa, A. Rodgers, J. Talati, Y. Lotan, *World J. Urol.*, 2017, **35**, 1301.

[5] M. Daudon, O. Traxer, P. Conort, B. Lacour, P. Jungers, *J. Am. Soc. Nephrol.*, 2006, **17**, 2026.

[6] M. Daudon, E. Letavernier, R. Weil, E. Véron, G. Matzen, G. André, D. Bazin, *C. R. Chim.*, 2016, **19**, 1527.

[7] K. Brandenburg, T. Schürholz, *World J. Biol. Chem.*, 2015, **6**, 71.

[8] L. N. Schultz, J. Connolly, E. Lauchnor, T. A. Hobbs, R. Gerlach, "Struvite Stone Formation by Ureolytic Biofilm Infections", in *The Role of Bacteria in Urology* (D. Lange, B. Chew, eds.), Springer International Publishing, Lausanne, 2016, 41-49.

[9] E. J. Espinosa-Ortiz, B. H. Eisner, D. Lange, R. Gerlach, *Nat. Rev. Urol.*, 2019, **16**, 35.

[10] M. Daudon, O. Traxer, E. Lechevallier, C. Saussine, *Prog. Urol.*, 2008, **18**, 802.

[11] J. E. Paonessa, E. Gnessin, N. Bhojanic, J. C. Williams Jr., J. E. Lingeman, *J. Urol.*, 2016, **196**, 769.

[12] J. Prywer, M. Olszynski, *Curr. Med. Chem.*, 2017, **24**, 292.

[13] D. O'Kane, A. Kiosoglous, K. Jones, *BMJ Case Rep.*, 2013, **2013**, article no. bcr2013009087.

[14] M. Daudon, C. A. Bader, P. Jungers, *Scanning Microsc.*, 1993, **7**, 1081.

[15] L. Maurice-Estepa, P. Levillain, B. Lacour, M. Daudon, *Scand. J. Urol. Nephrol.*, 1999, **33**, 299.

[16] H. M. Abrahams, M. L. Stoller, *Curr. Opin. Urol.*, 2003, **13**, 63.

[17] M. Daudon, P. Jungers, D. Bazin, *AIP Conf. Proc.*, 2008, **1049**, 199.

[18] M. Daudon, P. Jungers, D. Bazin, J. C. Williams Jr., *Urolithiasis*, 2018, **46**, 459.

[19] X. Carpentier, M. Daudon, O. Traxer, P. Jungers, A. Mazouyes, G. Matzen, E. Véron, D. Bazin, *Urology*, 2009, **73**, 968.

[20] M. Daudon, H. Bouzidi, D. Bazin, *Urol. Res.*, 2010, **38**, 459.

[21] K. M. Englert, J. A. McAteer, J. E. Lingeman, J. C. Williams Jr., *Urolithiasis*, 2013, **41**, 389.

[22] A. Hesse, H.-G. Tiselius, A. Jahnen (eds.), *Urinary Stones*, Karger, Basel, 2002.

[23] M. T. Gettman, J. W. Segura, *J. Endourol.*, 1999, **13**, 653.

[24] D. Bazin, G. André, R. Weil, G. Matzen, E. Véron, X. Carpentier, M. Daudon, *Urology*, 2012, **79**, 786.

[25] M. A. P. Manzoor, B. Singh, A. K. Agrawal, A. B. Arun, M. Mujeeburahiman, P. D. Rekha, *PLoS One*, 2018, **13**, article no. e0202306.

[26] P. Das, G. Gupta, V. Velu, R. Awasthi, K. Dua, H. Malipeddi, *Biomed. Pharmacother.*, 2017, **96**, 361.

[27] M. Daudon, *Archives de Pédiatrie*, 2000, **7**, 855.

[28] M. Daudon, A. Dessombz, V. Frochot, E. Letavernier, J. P. Haymann, P. Jungers, D. Bazin, *C. R. Chim.*, 2016, **19**, 1470.

[29] S. Reguer, C. Mocuta, D. Thiaudière, M. Daudon, D. Bazin, *C. R. Chim.*, 2016, **19**, 1424.

[30] D. Bazin, M. Daudon, *Ann. Biol. Clin.*, 2015, **73**, 517.

[31] D. Bazin, C. Jouanneau, S. Bertazzo, C. Sandt, A. Dessombz, M. Réfrégiers, P. Dumas, J. Frederick, J.-P. Haymann, E. Letavernier, P. Ronco, M. Daudon, *C. R. Chim.*, 2016, **19**, 1439.

[32] M. Daudon, D. Bazin, *J. Phys.: Conf. Ser.*, 2013, **425**, article no. 022006.

[33] D. Bazin, M. Daudon, *J. Phys. D: Appl. Phys.*, 2012, **45**, article no. 383001.

[34] D. Bazin, M. Daudon, C. Combes, C. Rey, *Chem. Rev.*, 2012, **112**, 5092.

[35] A. L. Rodgers, *Urolithiasis*, 2017, **45**, 27.

[36] M. Li, J. Zhang, L. Wang, B. Wang, C. V. Putnis, *J. Phys. Chem. B*, 2018, **122**, 1580.

[37] P. Chatterjee, A. Chakraborty, A. K. Mukherjee, *Spectrochim. Acta Part A*, 2018, **200**, 33.

[38] R. Gopal, C. Calvo, *Nat. Phys. Sci.*, 1972, **237**, 30.

[39] M. de Broglie, *C. R. Acad. Sci. Paris*, 1913, **157**, 924.

[40] M. Daudon, D. Bazin, "Application of physical methods to kidney stones and randall's plaque characterization", in *Urolithiasis* (J. Talati, H. G. Tiselius, D. Albala, Z. Ye, eds.), Springer, London, 2012.

[41] S. Rouzière, D. Bazin, M. Daudon, *C. R. Chim.*, 2016, **19**, 1404.

[42] D. Bazin, X. Carpentier, O. Traxer, D. Thiaudière, A. Somogyi, S. Reguer, G. Waychunas, P. Jungers, M. Daudon, *J. Synchrotron Rad.*, 2008, **15**, 506.

[43] D. Bazin, M. Daudon, P. Chevallier, S. Rouziere, E. Elkaim, D. Thiaudière, B. Fayard, E. Foy, P. A. Albouy, G. André, G. Matzen, E. Véron, *Ann. Biol. Clin.*, 2006, **64**, 125.

[44] X. Carpentier, D. Bazin, C. Combes, A. Mazouyes, S. Rouzière, P. A. Albouy, E. Foy, M. Daudon, *J. Trace Elements Med. Biol.*, 2011, **25**, 160.

[45] A. Dessombz, C. Nguyen, H. K. Ea, S. Rouzière, E. Foy, D. Hannouche, S. Réguer, F.-E. Picca, D. Thiaudière, F. Lioté, M. Daudon, D. Bazin, *J. Trace Elements Med. Biol.*, 2013, **27**, 326.

[46] D. Bazin, M. Daudon, *J. Spectral Imaging*, 2019, **8**, article no. a16.

[47] D. Bazin, D. A. Sayers, J. J. Rehr, *J. Phys. Chem. B*, 1997, **101**, 11040.

[48] D. Bazin, L. Guczi, J. Lynch, *App. Cat. A*, 2002, **226**, 87.

[49] M. T. D. Orlando, L. Kuplich, D. O. de Souza, H. Belich, J. B. Depianti, C. G. P. Orlando, E. F. Medeiros, P. C. M. da Cruz, L. G. Martinez, H. P. S. Corrêa, R. Ortiz, *Powder Diffr. Suppl.*, 2008, **23**, S59.

[50] D. Bazin, C. Chappard, C. Combes, X. Carpentier, S. Rouzière, G. André, G. Matzen, M. Allix, D. Thiaudière, S. Reguer, P. Jungers, M. Daudon, *Osteoporosis Int.*, 2009, **20**, 1065.

[51] T. Yapanoglu, A. Demirel, S. Adanur, H. Yüksel, O. Polat, *Turkish J. Med. Sci.*, 2010, **40**, 415.

[52] H. Almarshad, A. Alsharari, *J. Med. Imaging Health Inform.*, 2018, **8**, 655.

[53] M. Van Meerssche, J. Feneau-Dupont, *Introduction à la Cristallographie et à la Chimie Structurale*, Vander, Louvain, 1973.

[54] E. Bouderlique, E. Tang, J. Perez, A. Coudert, D. Bazin, M.-C. Verpont, C. Duranton, I. Rubera, J.-P. Haymann, G. Leftheriotis, L. Martin, M. Daudon, E. Letavernier, *Am. J. Pathol.*, 2019, **189**, 2171.

[55] J. Guerlain, S. Perie, M. Lefevre, J. Perez, S. Vandermeersch, C. Jouanneau, L. Huguet, V. Frochot, E. Letavernier, R. Weil, S. Rouzière, D. Bazin, M. Daudon, J. P. Haymann, *PLoS One*, 2019, **14**, article no. e0224138.

[56] E. Esteve, Y. Luque, J. Waeytens, D. Bazin, L. Mesnard, C. Jouanneau, P. Ronco, A. Dazzi, M. Daudon Deniset-Besseau, *Anal. Chem.*, 2020, **92**, 7388.

[57] D. Bazin, J.-P. Haymann, E. Letavernier, J. Rode, M. Daudon, *La Presse médicale*, 2014, **43**, 135.

[58] M. L. Giannossi, *J. X-Ray Sci. Technol.*, 2015, **23**, 401.

[59] E. Tsolaki, S. Bertazzo, *Materials*, 2019, **12**, 3126.

[60] N. Quy Dao, M. Daudon, *Infrared and Raman Spectra of Calculi*, Elsevier, Paris, 1997.

[61] L. Estepa, M. Daudon, *Biospectroscopy*, 1997, **3**, 347.

[62] M. Daudon, D. Bazin, *C. R. Chim.*, 2016, **19**, 1416.

[63] D. Bazin, E. Letavernier, J. P. Haymann, P. Méria, M. Daudon, *Progrès en Urol.*, 2016, **26**, 608.

[64] F. Brisset, M. Repoux, J. Ruste, F. Grillon, F. Robaut, *Microscopie Electronique à Balayage et Microanalyses*, EDP Sciences, France, 2009, ISBN: 978-2-7598-0082-7.

[65] M. Daudon, P. Junger, D. Bazin, *New England J. Med.*, 2008, **359**, 100.

[66] A. Dessombz, E. Letavernier, J.-P. Haymann, D. Bazin, M. Daudon, *J. Urol.*, 2015, **193**, 1564.

[67] E. Letavernier, G. Kauffenstein, L. Huguet, N. Navasiolava, E. Bouderlique, E. Tang, L. Delaitre, D. Bazin, M. de Frutos, C. Gay, J. Perez, M. C. Verpont *et al.*, *J. Am. Soc. Nephrol.*, 2018, **29**, 2337.

[68] H. Bilbault, J. Perez, L. Huguet, S. Vandermeersch, S. Placier, N. Tabibzadeh, V. Frochot, E. Letavernier, D. Bazin, M. Daudon, J.-P. Haymann, *Sci. Rep.*, 2018, **8**, 16319.

[69] D. Bazin, M. Daudon, E. Elkaim, A. Le Bail, L. Smrcok, *C. R. Chim.*, 2016, **19**, 1535.

[70] T. Roisnel, J. Rodriguez-Carvajal, *Mater. Sci. Forum*, 2001, **378–381**, 118.

[71] A. C. Larson, R. B. Von Dreele, *General Structure Analysis System (GSAS)*, vol. 86, Los Alamos National Laboratory Report LAUR, 2004.

[72] L. Borghi, A. Nouvenne, T. Meschi, *Nephr. Dial. Transpl.*, 2012, **27**, 3982.

[73] J. L. Bauza, E. C. Pieras, F. Grases, V. Tubau, J. Guimera, X. A. Sabate, P. Piza, *Med. Hypotheses*, 2018, **118**, 34.

[74] A. L. Schwaderer, A. J. Wolfe, *Ann. Transl. Med.*, 2017, **5**, 32.

[75] J. Prywer, M. Olszynski, E. M. Brzoska, *Cryst. Growth Des.*, 2017, **17**, 5953.

[76] J. Prywer, A. Torzewska, *Cryst. Growth Des.*, 2009, **9**, 3538.

[77] J. Prywer, R. Sadowski, A. Torzewska, *Cryst. Growth Des.*, 2015, **15**, 1446.

[78] J. Prywer, A. Torzewska, *Sci. Rep.*, 2019, **9**, 17061.

[79] S. B. Streem, G. Lammert, *J. Urol.*, 1992, **147**, 563.

[80] E. De Lorenzis, A. B. Alba, M. Cepeda, J. A. Galan, P. Geavlete, S. Giannakopoulos, I. Saltirov, K. Sarica, A. Skolarikos, S. Stavridis, E. Yuruk *et al.*, *Eur. J. Clin. Microbiol. Infect. Dis.*, 2020, **39**, 1971.

[81] A. R. Izatulina, A. M. Nikolaev, M. A. Kuz'mina, O. V. Frank-Kamenetskaya, V. V. Malyshev, *Crystals*, 2019, **9**, 259.

[82] R. Lagier, C. A. Baud, *Pathol. Res. Pract.*, 2003, **199**, 329.

[83] R. Scott, N. Stone, C. A. Kendall, K. Geraki, K. Rogers, *NPJ Breast Cancer*, 2016, **2**, 16029.

[84] A. Cariati, *Clin. Res. Hepatol. Gastroenterol.*, 2013, **37**, article no. e69.

[85] A. Dessombz, P. Méria, D. Bazin, E. Foy, S. Rouzière, M. Daudon, *Progrès en Urologie*, 2011, **21**, 940.

[86] A. Dessombz, P. Méria, D. Bazin, M. Daudon, *PLoS One*, 2012, **7**, article no. e51691.

[87] J. D. Reid, M. E. Andersen, *Atherosclerosis*, 1993, **101**, 213.

[88] F. A. Shah, B. E. J. Lee, J. Tedesco, C. L. Wexell, C. Persson, P. Thomsen, K. Grandfield, A. Palmquist, *Nano Lett.*, 2017, **17**, 6210.

[89] C. A. Scotchford, S. Y. Ali, *Ann. Rheum. Dis.*, 1995, **54**, 339.

[90] L. S. Burnstein, A. L. Boskey, P. J. Tannenbaum, A. S. Posner, I. D. Mandel, *J. Oral. Pathol.*, 1979, **8**, 284.

[91] A. Clifford, G. S. Hoffman, *Curr. Opin. Rheumatol.*, 2015, **27**, 397.

[92] J. Gervasoni, A. Primiano, P. M. Ferraro, A. Urbani, G. Gambaro, S. Persichilli, *J. Chem.*, 2018, article no. 4621256.

[93] J. Cloutier, L. Villa, O. Traxer, M. Daudon, *World J. Urol.*, 2015, **33**, 157.

[94] S. R. Khan, M. S. Pearle, W. G. Robertson, G. Gambaro, B. K. Canales, S. Doizi, O. Traxer, H.-G. Tiselius, *Nat. Rev. Dis. Primers*, 2016, **2**, 16008.

[95] M. Haddad, H. Vali, J. Paquette, S. R. Guiot, *PLoS One*, 2014, **9**, article no. e89480.

[96] C. Frondel, *Am. Mineral.*, 1941, **26**, 145.

[97] T. Debroise, E. Colombo, G. Belletti, J. Vekeman, Y. Su, R. Papoular, N. S. Hwang, D. Bazin, M. Daudon, P. Quaino, F. Tielens, *Cryst. Growth Des.*, 2020, **20**, 2553.

[98] C. Calvo, R. Gopal, *Am. Mineral.*, 1975, **60**, 120.

[99] D. Bazin, P. Chevallier, G. Matzen, P. Jungers, M. Daudon, *Urol. Res.*, 2007, **35**, 179.

[100] D. Bazin, X. Carpentier, I. Brocheriou, P. Dorfmuller, S. Aubert, C. Chappard, D. Thiaudière, S. Reguer, G. Waychunas, P. Junger, M. Daudon, *Biochimie*, 2009, **91**, 1294.

[101] E. Esteve, D. Bazin, C. Jouanneau, S. Rouzière, A. Bataille, A. Kellum, K. Provost, C. Mocuta, S. Reguer, P. Ronco, J. Rehr, J.-P. Haymann, E. Letavernier, A. Hertig, *C. R. Chim.*, 2016, **19**, 1580.

[102] E. Esteve, D. Bazin, C. Jouanneau, S. Rouzière, A. Bataille, A. Kellum, K. Provost, C. Mocuta, S. Reguer, P. Ronco, J. Rehr, J.-P. Haymann, E. Letavernier, A. Hertig, *C. R. Chim.*, 2016, **19**, 1586.

[103] R. M. Rousseau, *Spectrochim. Acta B*, 2006, **61**, 759.

[104] I. L. Thomas, M. T. Haukka, D. H. Anderson, *Anal. Chim. Acta*, 1979, **105**, 177.

[105] S. Kascakova, C. M. Kewish, S. Rouzière, F. Schmitt, R. Sobesky, J. Poupon, C. Sandt, B. Francou, A. Somogyi, D. Samuel, E. Jacquemin, A. Dubart-Kupperschmitt *et al.*, *J. Path.: Clin. Res.*, 2016, **2**, 175.

[106] E. Esteve, S. Reguer, C. Boissiere, C. Chanéac, G. Lugo, C. Jouanneau, C. Mocuta, D. Thiaudière, N. Leclercq, B. Leyh, J. F. Greisch, J. Berthault, M. Daudon, P. Ronco, D. Bazin, *J. Synchrotron Radiat.*, 2017, **24**, 991.

[107] H. D. Kim, H. L. Jang, N. Y. Ahn, H. K. Lee, J. Park, E.-S. Lee, E. A. Lee, Y.-H. Jeong, D.-G. Kim, K. T. Nam, N. S. Hwang, *Biomaterials*, 2017, **112**, 31.

[108] H. L. Jang, K. Jin, J. Lee, Y. Kim, S. H. Nahm, K. S. Hong, K. T. Nam, *ACS Nano*, 2014, **8**, 634.

[109] C. Millo, S. Dupraz, M. Ader, F. Guyot, C. Thaler, E. Foy, B. Ménez, *Geochim. Cosmochim. Acta*, 2012, **98**, 107.

[110] P. Scherrer, *Nachr Ges Wiss Göttingen*, 1918, **26**, 98.

[111] A. L. Patterson, *Phys. Rev.*, 1939, **56**, 978.

[112] D. Bazin, M. Daudon, G. André, R. Weil, E. Véron, G. Matzen, *J. Appl. Cryst.*, 2014, **47**, 719.

[113] H. Klug, L. Alexander, *X-Ray Diffraction Procedures for Polycrystalline and Amorphous Materials*, 2nd ed., Wiley, New York, 1974.

[114] S. Shaddel, S. Ucar, J. P. Andreassen, S. W. Østerhus, *J. Environ. Chem. Eng.*, 2019, **7**, article no. 102918.

[115] D. Jiao, C. King, A. Grossfield, T. A. Darden, P. Ren, *J. Phys. Chem. B*, 2006, **110**, 18553.

[116] H. H. Tuson, D. B. Weibel, *Soft Matter*, 2013, **9**, 4368.

[117] C. Cutinell, F. Galdiero, *J. Bacteriol.*, 1967, **93**, 2022.

[118] X. Yuntao, L. Yang, *Sci. Rep.*, 2016, **6**, 20628.

[119] K. Medjoubi, G. Baranton, A. Somogyi, *Microsc. Microanal.*, 2018, **24**, 252.

[120] F. Brunet-Possenti, L. Deschamps, H. Colboc, A. Somogyi, K. Medjoubi, D. Bazin, V. Descamps, *J. Eur. Acad. Derm. Venereol.*, 2018, **32**, article no. e442.

[121] T. Weitkamp, M. Scheel, J. Perrin, V. Le Roux, V. Joyet, S. Chaouchi, H. G. Pais, J.-L. Giorgetta *et al.*, *Microsc. Microanal.*, 2018, **24**, 244.